Nuclear Engineering and Design 310 (2016) 142–153

Contents lists available at ScienceDirect

Nuclear Engineering and Design

journal homepage: www.elsevier.com/locate/nucengdes

CFD modelling of hydrogen stratification in enclosures: Model validation and application to PAR performance

J.R. Hoyes *, M.J. Ivings

Health and Safety Laboratory, Buxton, UK

HIGHLIGHTS

- The ability of CFD to predict hydrogen stratification phenomena is investigated.
- Contrary to expectation, simulations on tetrahedral meshes under-predict mixing.
- Simulations on structured meshes give good agreement with experimental data.
- CFD model used to investigate the effects of stratification on PAR performance.
- Results show stratification can have a significant effect on PAR performance.

ARTICLE INFO

Article history:
Received 23 March 2016
Received in revised form 22 July 2016
Accepted 24 August 2016
Available online 26 October 2016

JEL classification:
K. Thermal Hydraulics

ABSTRACT

Computational Fluid Dynamics (CFD) models are maturing into useful tools for supporting safety analyses. This paper investigates the capabilities of CFD models for predicting hydrogen stratification in a containment vessel using data from the NEA/OECD SETH2 MISTRA experiments. Further simulations are then carried out to illustrate the qualitative effects of hydrogen stratification on the performance of Passive Autocatalytic Recombiner (PAR) units. The MISTRA experiments have well-defined initial and boundary conditions which makes them well suited for use in a validation study. Results are presented for the sensitivity to mesh resolution and mesh type. Whilst the predictions are shown to be largely insensitive to the mesh resolution they are surprisingly sensitive to the mesh type. In particular, tetrahedral meshes are found to induce small unphysical convection currents that result in molecular diffusion and turbulent mixing being under-predicted. This behaviour is not unique to the CFD model used here (ANSYS CFX) and furthermore, it may affect simulations run on other non-aligned meshes (meshes that are not aligned perpendicular to gravity), including non-aligned structured meshes. Following existing best practice guidelines can help to identify potential unphysical predictions, but as an additional precaution consideration should be given to using gravity-aligned meshes for modelling stratified flows. CFD simulations of hydrogen recombination in the Becker Technologies THAI facility are presented with high and low PAR positions and homogeneous and stratified initial hydrogen distributions. For the stratified initial hydrogen distribution, as expected, the high PAR location performs better than the low positioned PAR. However, for the homogeneous initial hydrogen distribution, the low PAR location performs better than the high PAR. The work demonstrates that CFD can be a useful tool to help inform the positioning of PAR units, which may provide a practicable risk-reduction measure for situations where hydrogen releases are possible.

1. Introduction

The Fukushima Daiichi accident serves as a recent reminder of the potential consequences of the release and ignition of hydrogen during accident conditions in a nuclear power plant. The accident occurred in March 2011 when a magnitude 9.0 earthquake led to a loss of mains power and triggered a tsunami that breached the plant's seawall and damaged diesel generators (NEA, 2013). Cooling systems were temporarily powered by emergency batteries but when these were depleted overheating led to a reaction between zirconium fuel-cladding and water that generated hydrogen. The hydrogen was released into the reactor buildings where it mixed with air and ultimately led to a series of explosions that

* Corresponding author.
E-mail address: james.hoyes@hsl.gsi.gov.uk (J.R. Hoyes).

http://dx.doi.org/10.1016/j.nucengdes.2016.08.036
0029-5493/

caused significant damage to the nuclear power plant (TEPCO, 2012; NRA, 2014).

Oxidation of metal cladding also represents a hazard in other nuclear facilities. For example, used magnox cladding from first generation UK nuclear power plants stored under water continues to oxidise and generate hydrogen (Sellafield, 2015). Following the Fukushima Daiichi accident, the EC initiated a programme of "Stress Tests" to review the resilience of nuclear facilities to severe accident scenarios (EC, 2012). The UK actively participated in this initiative and identified a number of areas for improvement (ONR, 2012).

Fukushima also led to an increase in interest in work on hydrogen explosions (NEA, 2011) and motivated further work to develop and validate Lumped Parameter (LP) and Computational Fluid Dynamics (CFD) models. These models can be used to predict the consequences of a postulated accident (Kljenak et al., 2013; Hoyes et al., 2013; Sathiah et al., 2015) and to help analyse accidents that have occurred (Kuznetsov et al., 2015). Additionally, Fukushima led to an increase in interest in mitigation strategies including hydrogen igniters, filtered containment venting, Passive Autocatalytic Recombiner (PAR) units (Gupta, 2015) and passive ventilation (Hedley et al., 2014).

The consequences of a hydrogen explosion and the design of mitigation strategies depend on the dispersion and accumulation behaviour of the hydrogen. For example, a stratified distribution could lead to locally higher hydrogen concentrations, which could in turn lead to flame acceleration and higher explosion overpressures (Hooker et al., 2015). Similarly, knowledge of the hydrogen distribution can be used to inform the positioning of hydrogen mitigation equipment including igniters and PAR units.

The dispersion behaviour will depend on the characteristics of the release and the geometry of the enclosure (Agrawal et al., 2015). Furthermore, other gas releases or flows associated with mitigation strategies could affect the hydrogen distribution. Physical modelling is often restricted to relatively small-scale scenarios and, for safety reasons, it is often carried out using helium as a surrogate for hydrogen. Historically, analytical calculations and LP codes have been used to predict hydrogen dispersion, whilst more recently the use of CFD codes has become more widespread. CFD codes offer greater potential for predicting hydrogen stratification phenomena compared to LP codes that have "limited" ability to predict stratification and integral codes that have "very limited" ability to predict stratification (IAEA, 2011). However, there is an on-going need to provide validation of CFD codes before they can be relied upon (Paladino et al., 2012).

The first part of this paper describes the validation of a CFD model (ANSYS CFX) against measurements from experiments carried out for the second SESAR Thermal-Hydraulics (SETH2) project (NEA, 2012). The SETH2 project was coordinated by the Nuclear Energy Agency (NEA) of the Organisation for Economic Cooperation and Development (OECD) and it sought to build on work into the formation of stratified layers (NEA, 2007) by investigating the mixing of stratified helium-rich layers by molecular and turbulent diffusion. Experiments for SETH2 were carried out using the Commissariat à l'Energie Atomique (CEA) MISTRA and Paul Scherrer Institute (PSI) PANDA test facilities. Four MISTRA tests were selected for model validation covering stratification phenomena in the presence of convection currents with different strengths from no convection (molecular diffusion only) to dominant convection (high momentum air jet). The MISTRA experiments are described in Section 2, the modelling approach is described in Section 3 and the results of the validation study are described in Section 4.

In the second part of this paper, the model is used as a tool to study a number of hypothetical scenarios in which a PAR unit is used to reduce the quantity of hydrogen in an enclosure. PAR units contain catalysts that can recombine hydrogen and oxygen into steam and heat at relatively low hydrogen concentrations of around 0.01 v/v – i.e. well below the lower flammability limit for hydrogen of around 0.04 v/v (Lewis and von Elbe, 1961). They are passive safety systems in that they do not rely on an external power source or operator control, but are instead driven by natural convection. The German Reactor Safety Commission (RSK) has recommended the installation of PAR units in German Pressurized Water Reactor (PWR) containment buildings since 1994 (Allelein et al., 2008). Conversely, the UK has only limited experience with PAR units, in part because most operating UK nuclear power plants are gas-cooled (rather than water-cooled) and are therefore, less susceptible to hydrogen generation. However, up to 47 PAR units are included in the proposed UK-EPR reactor design (ONR, 2011) and following the EU Stress Tests, PAR units will be retro-fitted to the UK's existing PWR, Sizewell B (ONR, 2012). Section 5 describes the application of the validated model to PAR performance, the results are presented and discussed in Section 6 and finally, conclusions are drawn in Section 7.

2. Overview of the MISTRA experiments

The MISTRA test facility consists of a large cylindrical vessel with an internal height of 7.4 m and an internal diameter of 4.3 m (Studer et al., 2012). It has a flat ceiling and a hemi-ellipsoidal floor and for the tests described here, it was configured with an inner cylinder, ring plate, vent and air-jet nozzle. The set-up is shown in Fig. 1: the inner cylinder had a height of 4.2 m, a diameter of 1.9 m and was positioned 1.2 m above the vessel floor; the ring plate had a diameter of 3.5 m and was 3.7 m above the floor; the vent had a diameter of 200 mm and was 2.0 m above the floor and the air-jet nozzle was vertically orientated, had a diameter of 72 mm and was attached to the ring plate, 1.4 m from the centre-axis of the vessel. Ten katharometer gas concentration sensors (with a measurement uncertainty of 5%) were positioned in the top 2.4 m of the vessel (Brinster et al., 2011).

The tests involved first releasing helium to establish a stratified layer in the top of the vessel. Helium was used as a surrogate for hydrogen for safety reasons and because it has similar buoyancy and diffusivity characteristics. Fig. 2 shows target and measured helium distributions. The target helium distribution was a uniform 0.4 v/v in the top 1 m of the vessel. However, mixing during the release phase meant that actual helium concentrations varied from 0.4 v/v near the top of the vessel to zero 1.7 m below the ceiling. A concentration of 0.4 v/v represents a fairly rich mixture compared to, for example, the stoichiometric concentration of hydrogen in air of 0.3 v/v (Lewis and von Elbe, 1961).

Once the helium-rich layer had been established, measurements were made of the rate at which it mixed with the air in the rest of the vessel. Table 1 summarises the key characteristics of four tests that were selected for model validation. The INITIALA_3 test involved mixing by molecular diffusion only whereas the two LOWMA_3 tests and the LOWMA_4 test all involved mixing by molecular diffusion and air jets[1] (introduced through the 72 mm diameter nozzle). The two LOWMA_3 tests were selected to illustrate the repeatability of the measurements. They had nominally identical air jet mass release rates of 15.2 g/s (corresponding to a velocity of 3.1 m/s), however, there were some differences in temperature due to the tests being carried out on different days. In LOWMA_3a the air jet and vessel gas had approximately the same temperature whereas in LOWMA_3b the air jet was about 4 °C colder

[1] The air jets introduce momentum and lead to momentum-driven mixing (also referred to as turbulent diffusion as the mixing is caused by turbulence generated by the fluid momentum).

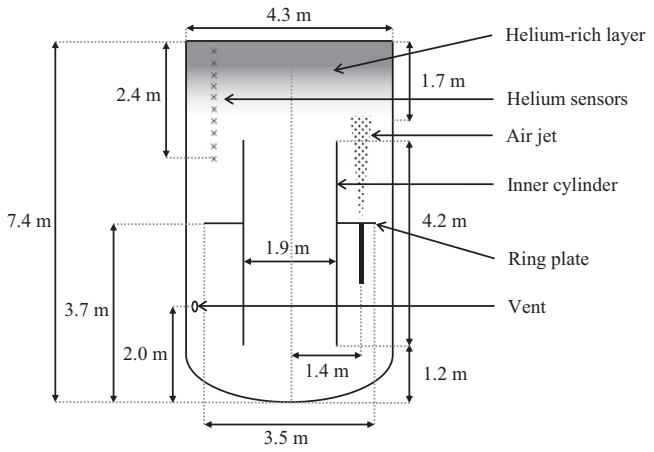

Fig. 1. Schematic of the MISTRA facility showing the inner cylinder, ring plate, air jet, vent and helium katharometer sensors (Brinster et al., 2011; Studer et al., 2012).

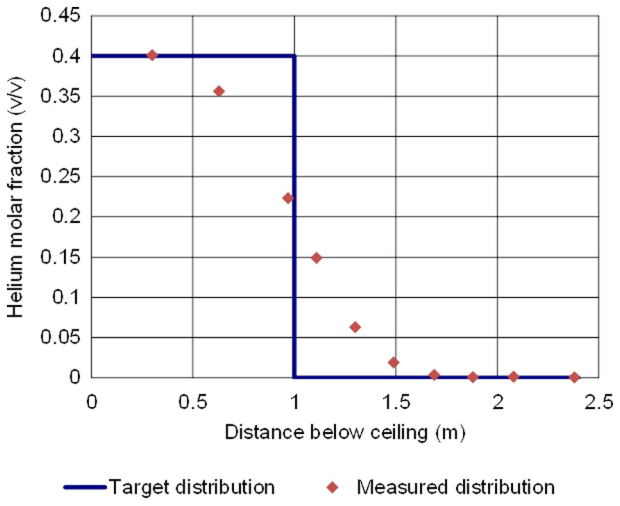

Fig. 2. Target and measured helium distributions at the end of the helium release phase (Brinster et al., 2009; Studer et al., 2012).

than the gas initially in the vessel. The LOWMA_4 test had a higher air jet mass release rate of 50.6 g/s (corresponding to a velocity of 10.2 m/s).

Studer et al. (2012) used two similar but different interaction Froude numbers to characterise the behaviour of the air jets. The first interaction Froude number, Fr_1, describes whether or not the air jet penetrates the buoyant helium-rich layer whilst the second Froude number, Fr_2, describes whether or not it penetrates the full depth of the buoyant helium-rich layer. If $Fr_1 < 1$ the air jet will not have enough inertia to reach the stratified layer, whereas if $Fr_1 > 1$ it will reach and penetrate the stratified layer. Similarly, if $Fr_2 < 1$ the air jet will not penetrate the full depth of the stratified layer, whereas if $Fr_2 > 1$ the air jet will penetrate the full depth of the stratified layer. According to the interaction Froude number analyses, the LOWMA_3 and LOWMA_4 tests represent the interesting cases of the air jet just reaching the stratified layer and the air jet penetrating almost the full depth of the stratified layer, respectively.

Helium concentration measurements from INITIALA_3 are shown in Fig. 3 at various heights below the ceiling. They show the buoyant helium-rich layer slowly mixing with the air in the rest of the vessel. The helium concentration 0.3 m below the ceiling decreases from 0.4 v/v at the start of the test to 0.23 v/v after 10,000 s. Helium concentrations at 0.65 m and 0.95 m also decrease, however, at 1.1 m and below the concentrations increase as helium diffuses from high concentration regions to low concentration regions. The helium concentration 1.7 m below the ceiling increases from zero to 0.11 v/v after 10,000 s.

Corresponding helium concentration measurements from the two LOWMA_3 tests are shown in Figs. 4 and 5. The two tests have similar helium distributions at time zero and they both show a faster rate of mixing than the INITIALA_3 test. Furthermore, the two LOWMA_3 tests exhibit similar behaviour before and after the air jet is turned off at 6000 s. There are however some differences between the two LOWMA_3 tests. In LOWMA_3a the air jet penetrates the buoyant helium-rich layer to a depth of 1.1 m below the ceiling and homogenises the region between 1.1 m and 2.4 m below the ceiling. Conversely, in LOWMA_3b the air jet has a reduced penetration depth and homogenises the region between 1.5 m and 2.4 m below the ceiling. The differences are thought to be caused by the small temperature differences shown in Table 1 (Brinster et al., 2009). After the air jets are turned off at 6000 s, the homogenised regions both regain stratified distributions. This occurs as helium diffuses from high to low concentration regions, as observed in the INITIALA_3 test.

Measurements from the LOWMA_4 test are shown in Fig. 6. The rate of mixing is much faster than in either the INITIAL_3 or LOWMA_3 tests and consequently, measurements are only shown for the first 1000 s. During the first 300 s the concentration measurements converge to 0.11 v/v, as the air jet very quickly homogenises the region covered by the sensors. During the following 700 s the concentration in this region decreases from 0.11 v/v to 0.06 v/v.

Further details of the MISTRA experiments can be found in Brinster et al. (2009, 2011) and Studer et al. (2012). The data generated provide a useful resource for model validation. Although not discussed here, a number of additional tests were carried out to confirm the repeatability of the measurements. Furthermore, a number of simple yet pragmatic checks were carried out to substantiate the measurements, including checks for mass conservation.

3. Modelling approach

CFD modelling of the MISTRA tests was carried out using the commercially available code ANSYS CFX (ANSYS, 2011). This Section describes the modelling approach; including the model geometry, computational mesh, choice of sub-models, boundary and initial conditions, and solution procedure, and highlights the main simplifications and assumptions used. Note that the choice of assumptions reflects the fact that the purpose of the work was

Table 1
Summary of the MISTRA experiments selected for model validation.

Test	Air jet mass flow rate (g/s)	$T_{initial}$–T_{jet} (°C)	Air jet duration (s)	Interaction Froude number (Fr_1)	Interaction Froude number (Fr_2)
INITIALA_3	n/a	n/a	n/a	0	0
LOWMA_3a	15.2	≈0	6000	1.00	0.29
LOWMA_3b	15.2	≈4	6000	1.00	0.29
LOWMA_4	50.6	n/a	5400	3.35	0.96

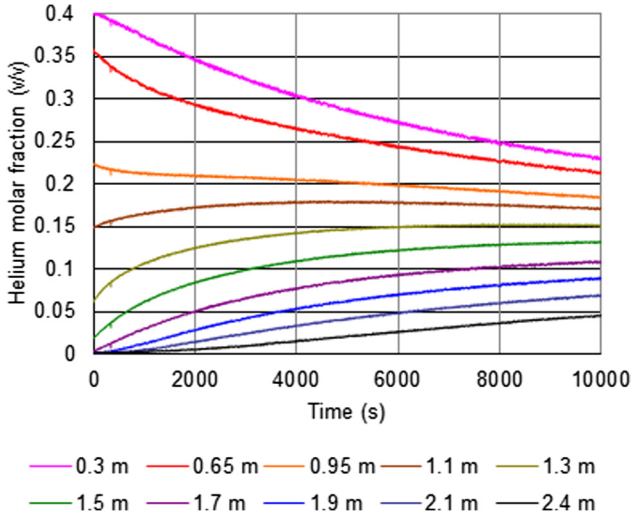

Fig. 3. Helium concentration measurements from INITIALA_3 coloured by distance below ceiling (Brinster et al., 2009; Studer et al., 2012). (For interpretation of the references to colour in this figure legend, the reader is referred to the web version of this article.)

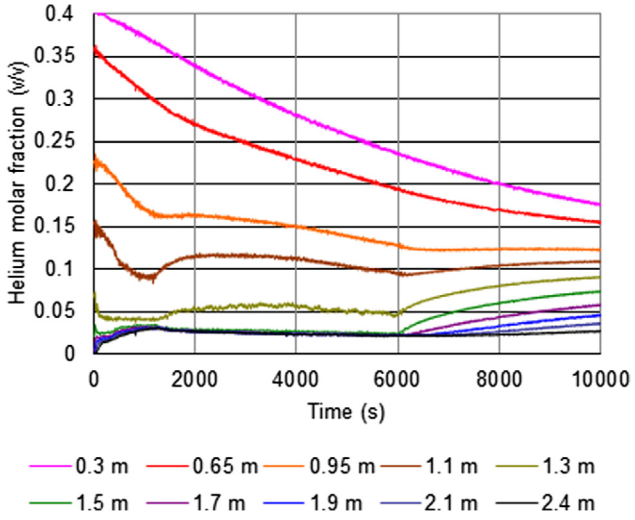

Fig. 4. Helium concentration measurements from LOWMA_3b, coloured by distance below ceiling (Brinster et al., 2009; Studer et al., 2012). (For interpretation of the references to colour in this figure legend, the reader is referred to the web version of this article.)

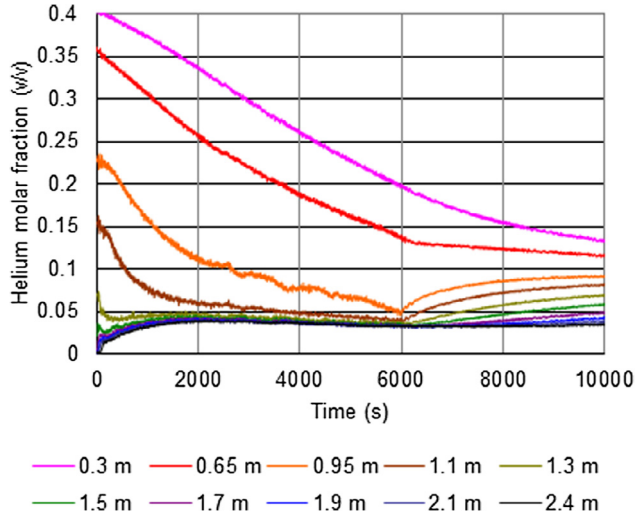

Fig. 5. Helium concentration measurements from LOWMA_3a, coloured by distance below ceiling (Brinster et al., 2009; Studer et al., 2012). (For interpretation of the references to colour in this figure legend, the reader is referred to the web version of this article.)

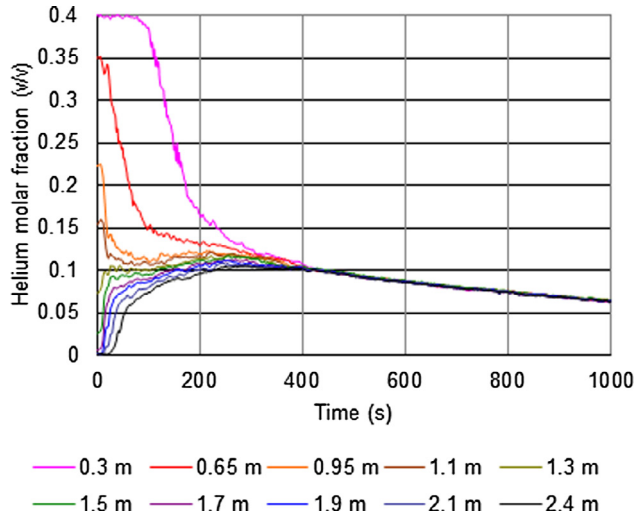

Fig. 6. Helium concentration measurements from LOWMA_4 coloured by distance below ceiling (Brinster et al., 2009; Studer et al., 2012). (For interpretation of the references to colour in this figure legend, the reader is referred to the web version of this article.)

model validation. If the work had been carried out for a safety case, a greater level of emphasis would have been placed on the use of conservative assumptions.

The model geometry consists of a cylindrical volume with a diameter and height that were chosen to match the experimental set-up. The geometry used for the LOWMA simulations also includes the open 0.2 m diameter vent for maintaining atmospheric pressure and a 72 mm diameter pipe for releasing air jets. The inner cylinder and ring plate weren't modelled as preliminary simulations indicated that they had little effect on the phenomena being simulated and excluding them meant that it was easier to construct the computational mesh.

Simulations were carried out using a tetrahedral mesh and medium and fine resolution structured meshes. While structured meshes tend to be more accurate and more computationally efficient, tetrahedral meshes offer greater flexibility in terms of resolving geometrical features and specifying local mesh refinement. The medium and fine resolution structured meshes had 0.7 and 1.2 million nodes and resolutions on the jet orifice of 0.01 m and 0.006 m, respectively. The tetrahedral mesh had a similar resolution on the jet orifice to the medium resolution structured mesh but a higher cell count of 1 million nodes.

The tetrahedral and medium resolution structured meshes used for the LOWMA simulations are shown in Fig. 7. The meshes have local mesh refinement near the interface between helium-rich and helium-lean regions and along the path of the air jets. The structured mesh includes some tetrahedral elements in the bottom of the vessel. These were used to resolve the ellipsoidal bottom surface and the circular vent. Similar meshing schemes were used for the INITIALA_3 simulations.

Conservation of fluid mass and momentum were modelled using the Navier-Stokes equations, whilst the helium distribution was modelled using a scalar transport equation for the helium mass fraction:

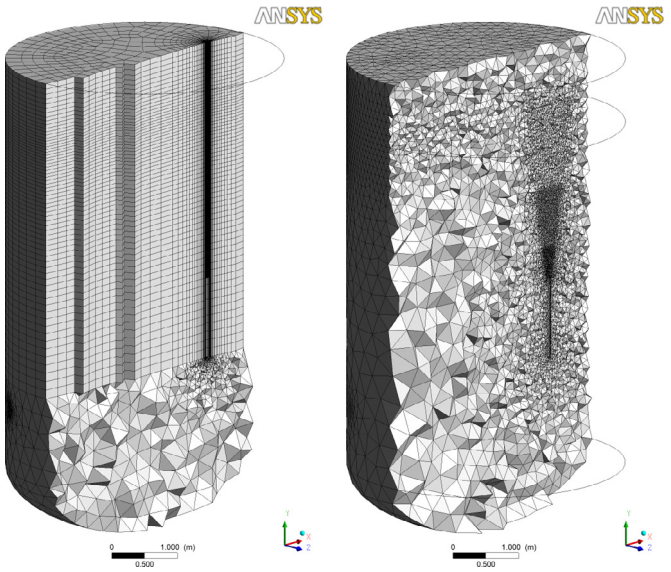

Fig. 7. Structured (left) and tetrahedral (right) meshes used for the LOWMA simulations.

$$\frac{\partial(\rho\omega_{He})}{\partial t} + \nabla\cdot(\rho U\omega_{He}) = \nabla\cdot\left(\left(\rho D + \frac{\mu_t}{Sc_t}\right)\nabla\omega_{He}\right) \quad (1)$$

where ρ is the fluid density, ω_{He} is the helium mass fraction, t is time, U is the fluid velocity, μ_t is the turbulent viscosity and Sc_t is the turbulent Schmidt number. The molecular diffusivity coefficient for helium in air, D, was set to 6.86×10^{-5} m^2/s (Bird et al., 1960).

The simulations were carried out using the k–ε turbulence model and included the effects of buoyancy on turbulence production and dissipation (Visser et al., 2012). Temperature variations were neglected as INITIALA_3 and LOWMA_3a were nearly isothermal and LOWMA_4 was insensitive to small temperature variations.

The vessel walls were modelled as no-slip hydraulically smooth walls, the vent was modelled as a pressure opening and the air jets were modelled as inlets with high intensity turbulence of 10% (ANSYS, 2011), a uniform velocity profile and a mass flow rate chosen to match the experimental conditions. At time zero the velocity was set to zero, the turbulence intensity was set to low intensity of 1% (ANSYS, 2011) and the helium distribution was set to match the measured helium distribution, with linear interpolation between the discrete measurement points.

The simulations were carried out using 'high resolution' discretisation in space and second order discretisation in time (ANSYS, 2011). The simulations were judged to have converged when normalised Root Mean Square (RMS) residual values reached the recommended values of 10^{-4} or less.

4. Model validation

This section describes the validation of the CFD model using the MISTRA measurements described in Section 2. The aims were to provide confidence in the model's ability to predict stratification phenomena relevant to the use of a PAR unit and more generally, to provide insight into the use of CFD for safety analyses.

The model is validated against the measurements from the LOWMA_3a test and then against the measurements from the INITIALA_3 and LOWMA_4 tests. The validation against LOWMA_3a includes simulations to assess the sensitivity of the model to the mesh resolution and mesh type. Predictions for LOWMA_3a are also compared to data from LOWMA_3b, for comparison purposes. Table 2 provides an overview of the simulations and a summary of whether or not they provided qualitative and quantitative agreement with the measurements.

Note that a number of simulations were carried out in addition to those shown in Table 2, including simulations to assess the sensitivity of the model to the use of a single or double precision solver, the RMS convergence criteria, the use of isothermal conditions and the choice of turbulence model. Furthermore, simulations of molecular diffusion were carried out and compared to an analytical solution and simulations of the PSI PANDA tests were carried out and compared to measurements in Studer et al. (2012). Whilst these additional simulations are not described here they helped inform and provide confidence in the set of analyses presented.

Helium concentration predictions from simulation MV1 of LOWMA_3a are shown in Fig. 8. They show the maximum concentration decreasing from 0.4 v/v to 0.2 v/v as the helium-rich layer mixes with the air in the rest of the vessel. The predictions also show the air jet reaching the bottom of the helium-rich layer but not significantly penetrating it. This is in qualitative agreement with the Froude number analysis of Studer et al. (2012).

The predictions from simulation MV1 are compared to the measurements from LOWMA_3a in Fig. 9. They show qualitatively similar behaviour before and after the air jet is turned off at 6000 s and overall, they are in reasonable quantitative agreement with the measurements. Most of the predictions are within 0.04 v/v of the measurements.

Predictions from MV2 and MV3 are shown in Figs. 10–12 at 0.65 m, 1.1 m and 1.5 m below the ceiling, respectively. Also shown in these Figures are the MV1 predictions and the measurements from both LOWMA_3 tests. Whilst the predictions from MV1 and MV2 are in reasonable agreement with each other and with the measurements, the predictions from MV3 are significantly different.

Fig. 10 shows that MV3 over-predicts the helium concentration at 0.65 m, whilst Fig. 11 shows that it under-predicts it at 1.1 m. The MV3 predictions are presented in Fig. 13, which shows the interface between helium-rich and helium-lean gases getting sharper and the concentration in the top of the vessel increasing. This behaviour is qualitatively different to that observed in either LOWMA_3 test. It was found to be caused by the tetrahedral mesh, which induced small, unphysical, buoyancy-driven convection currents that counteracted molecular diffusion and turbulent mixing. Correspondence with ANSYS revealed that this unphysical behaviour is not unique to the version of CFX used here and that it could occur in simulations run on other non-aligned meshes (meshes that are not aligned perpendicular to gravity), including non-aligned structured meshes. Other CFD codes could also be affected.

In more complex flows this effect may be relatively subtle and therefore overshadowed by other flow features making it more difficult to spot. However, following existing best practice guidelines should help to identify any such unphysical behaviour. For example, NEA (2015) recommends a mesh sensitivity analysis be carried out using at least two meshes with significantly different resolutions. In this instance the behaviour was sensitive to the mesh resolution – simulations on course and fine resolution tetrahedral meshes gave results that were significantly different to each other as well as being different to the measurements. Furthermore, NEA (2015) recommends adopting a tiered approach to model validation in which separate effect phenomena are considered. In this case simulations of molecular diffusion can be carried out and predictions compared to an analytical[2] solution (Crank, 1975):

[2] Eq. (2) is referred to as an analytical solution but in practice it is evaluated numerically – with infinity replaced by a large but finite number.

Table 2
Overview of CFD model validation simulations and predictions.

Simulation	Test simulated	Mesh resolution	Mesh type	Qualitative and quantitative agreement with measurements?
MV1	LOWMA_3a	Medium	Structured	Yes
MV2	LOWMA_3a	Fine	Structured	Yes
MV3	LOWMA_3a	Medium	Tetrahedral	No
MV4	INITIALA_3	Medium	Structured	Yes
MV5	LOWMA_4	Medium	Structured	Yes

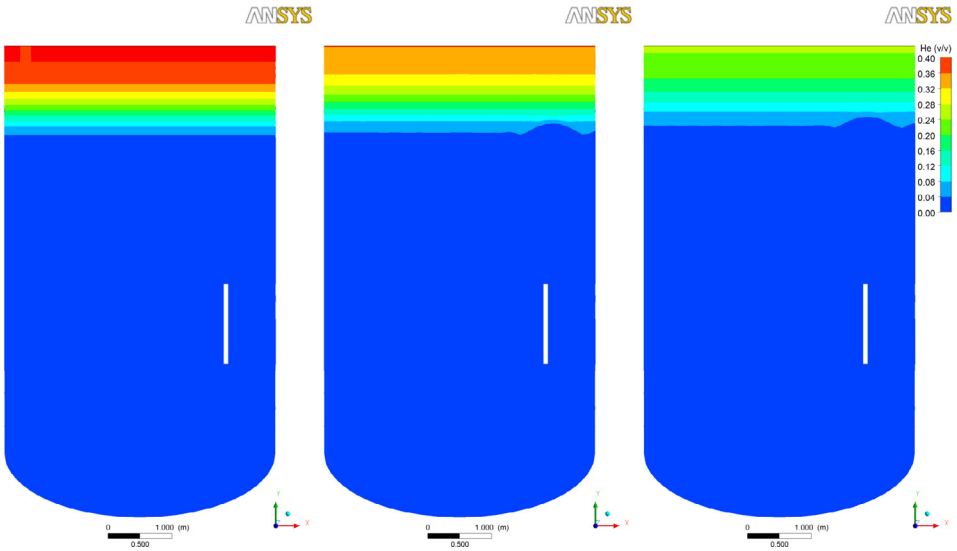

Fig. 8. Centre plane helium concentration predictions from simulation MV1 of LOWMA_3a at t = 0, 1800 and 6000 s (left to right).

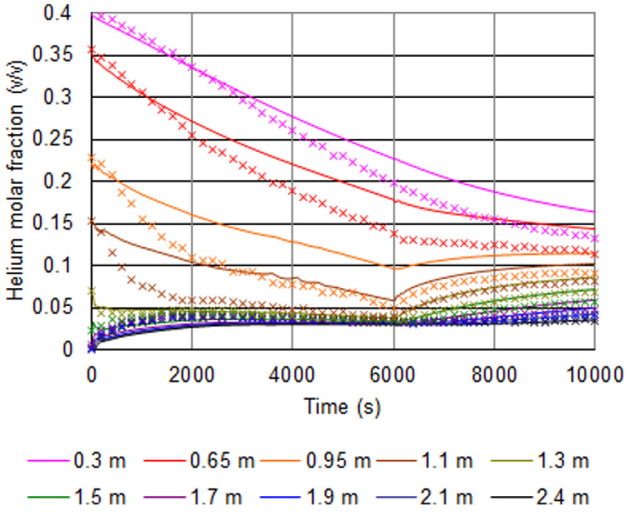

Fig. 9. Helium concentration measurements from LOWMA_3a (crosses) and CFD predictions from MV1 (lines).

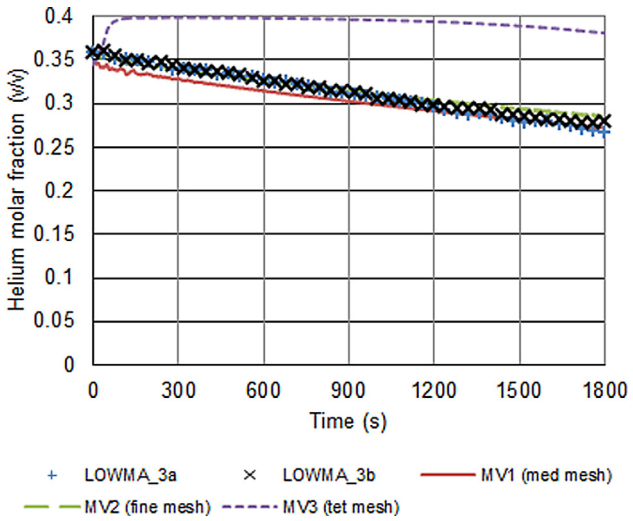

Fig. 10. Helium concentration measurements from LOWMA_3 tests and CFD predictions 0.65 m below the ceiling.

$$c_{He} = c_{He,0}\left\{\frac{h}{l} + \frac{2}{\pi}\sum_{n=1}^{\infty}\sin\left(\frac{n\pi h}{l}\right)\exp\left(-\frac{n^2\pi^2}{l^2}Dt\right)\cos\left(\frac{n\pi y}{l}\right)\right\} \quad (2)$$

where c_{He} is the helium molar fraction, $c_{He,0}$ is the helium molar fraction at time zero, h is the initial height of the helium stratification, l is the height of the vessel and y is the vertical coordinate.

In light of the issue described above, only predictions from simulations carried out using gravity-aligned structured meshes are presented for the INITIALA_3 and LOWMA_4 tests. However, prior to presenting these predictions, it is of interest to note that simulations of INITIAL_3 and LOWMA_4 were carried out using tetrahedral meshes and that whilst the LOWMA_4 predictions were in reasonable agreement with the measurements (perhaps because LOWMA_4 is sufficiently momentum dominated), the INITIAL_3 simulation on a tetrahedral mesh showed similar unphysical behaviour to that observed in MV3.

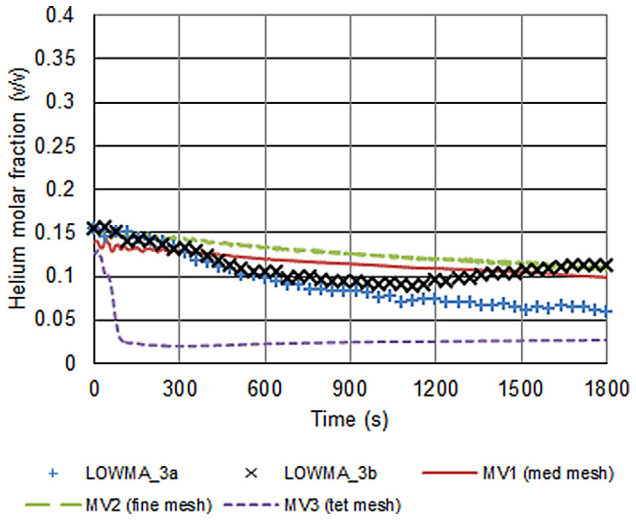

Fig. 11. Helium concentration measurements from LOWMA_3 tests and CFD predictions 1.1 m below the ceiling.

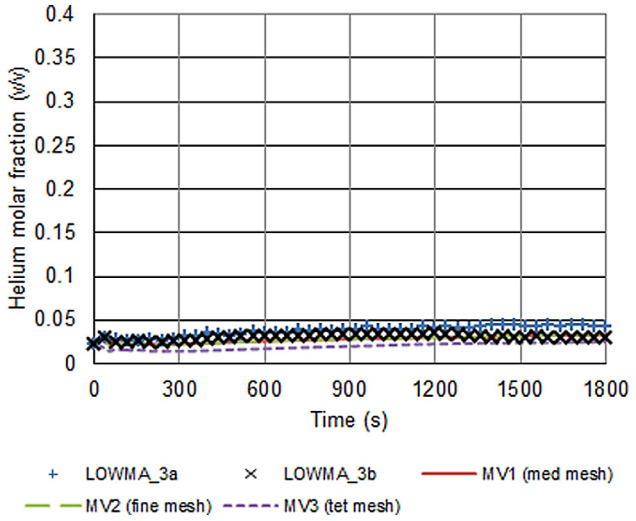

Fig. 12. Helium concentration measurements from LOWMA_3 tests and CFD predictions 1.5 m below the ceiling.

Figs. 14–17 show predictions of INITIALA_3 and LOWMA_4 from simulations carried out using gravity-aligned structured meshes. The INITIALA_3 predictions show a relatively slow rate of mixing compared to the LOWMA_3 predictions, whereas the LOWMA_4 predictions show a relatively fast rate of mixing. The LOWMA_4 predictions also show the air jet penetrating the full depth of the stratified layer, as predicted by the Froude number analysis of Studer et al. (2012).

The INITIALA_3 and LOWMA_4 predictions are in good agreement with the corresponding measurements. The level of agreement is generally better than that observed for LOWMA_3 with most of the predictions lying within 0.02 v/v of the measurements. The balance between molecular and turbulent mixing present in LOWMA_3 appears to represent the most challenging case for the CFD model.

5. Application to PAR performance

The validation study presented above provides confidence in the ability of the CFD model to predict stratification phenomena in the presence of different strength convection currents. In this Section the model is used to investigate the possible effects of stratification on the performance of a PAR unit and illustrate the ability of CFD to provide data on this. While these simulations introduce new physics that weren't covered within the validation exercise, the approach that has been used follows the work and conclusions from Visser et al. (2012).

A series of hypothetical scenarios were simulated in which hydrogen in the THAI facility (Gupta, 2015) was recombined using a half FR1-380 PAR unit (AREVA, 2011). This section describes the THAI geometry and the approach used to model the PAR unit. The modelling approach was based on the MISTRA validation study and included using gravity-aligned meshes. Temperature effects on buoyancy were modelled using the full-buoyancy model (ANSYS, 2011). The results are presented and discussed in Section 6.

Fig. 18 shows the THAI vessel and PAR unit. The THAI vessel is 9.2 m high and 3.2 m in diameter and the PAR unit is 1.4 m high, 0.3 m deep and 0.2 m wide. The PAR unit has an inlet on its bottom surface and an outlet on its side walls and was located either 2 m (low position) or 6 m (high position) above the vessel floor.

PAR modelling approaches vary in complexity depending on the application. For example, Meynet and Bentaib (2012) used a very detailed model (called SPARK) to investigate ignition phenomena caused by hot catalyst surfaces, whereas Kudriakov et al. (2008) used a relatively simple model to investigate large-scale thermal-hydraulic processes in a simulated containment building. The approach used here is similar to that described by Kudriakov et al. (2008) and involved defining the mass flow rate at the inlet and the mass flow rate, temperature and hydrogen, oxygen and water mass fractions at the outlet.

The mass flow rate at the inlet was defined as:

$$\dot{m}_{\mathrm{in}} = \frac{\dot{r}_{\mathrm{H2}}}{\varepsilon_{\mathrm{PAR}}\omega_{\mathrm{H2in}}} \tag{3}$$

where $\dot{r}_{\mathrm{H2}}$ is the recombination rate (the mass of hydrogen recombined per unit time, see below), $\varepsilon_{\mathrm{PAR}}$ is the PAR efficiency (the fraction of hydrogen entering the PAR that is recombined) and ω_{H2in} is the hydrogen mass fraction at the inlet. The efficiency for a half FR-380 PAR unit is typically between 0.4 to 0.55 (Kanzleiter, 2009) and a value of 0.4 was used here.

Conservation of mass means the mass flow rate at the outlet must equal the mass flow rate at the inlet:

$$\dot{m}_{\mathrm{out}} = \dot{m}_{\mathrm{in}} \tag{4}$$

The hydrogen, oxygen and water mass fractions at the outlet are related to their values at the inlet, taking into account the recombination of hydrogen and oxygen into steam inside the PAR unit, as follows:

$$\omega_{\mathrm{H2out}} = \omega_{\mathrm{H2in}} - \frac{\dot{r}_{\mathrm{H2}}}{\dot{m}_{\mathrm{in}}} \tag{5}$$

$$\omega_{\mathrm{O2out}} = \omega_{\mathrm{O2in}} - \frac{M_{\mathrm{O2}}}{2M_{\mathrm{H2}}}\frac{\dot{r}_{\mathrm{H2}}}{\dot{m}_{\mathrm{in}}} \tag{6}$$

$$\omega_{\mathrm{H2Oout}} = \omega_{\mathrm{H2Oin}} + \frac{M_{\mathrm{H2O}}}{M_{\mathrm{H2}}}\frac{\dot{r}_{\mathrm{H2}}}{\dot{m}_{\mathrm{in}}} \tag{7}$$

where M_{O2}, M_{H2} and M_{H2O} are the molecular weights of oxygen, hydrogen and water.

The relationship between the outlet and inlet gas temperatures, taking into account the heat released by the recombination process, is given by:

$$T_{\mathrm{out}} = T_{\mathrm{in}} + \frac{\Delta H_{\mathrm{H2}}}{cp_{\mathrm{in}}}\frac{\dot{r}_{\mathrm{H2}}}{\dot{m}_{\mathrm{in}}} \tag{8}$$

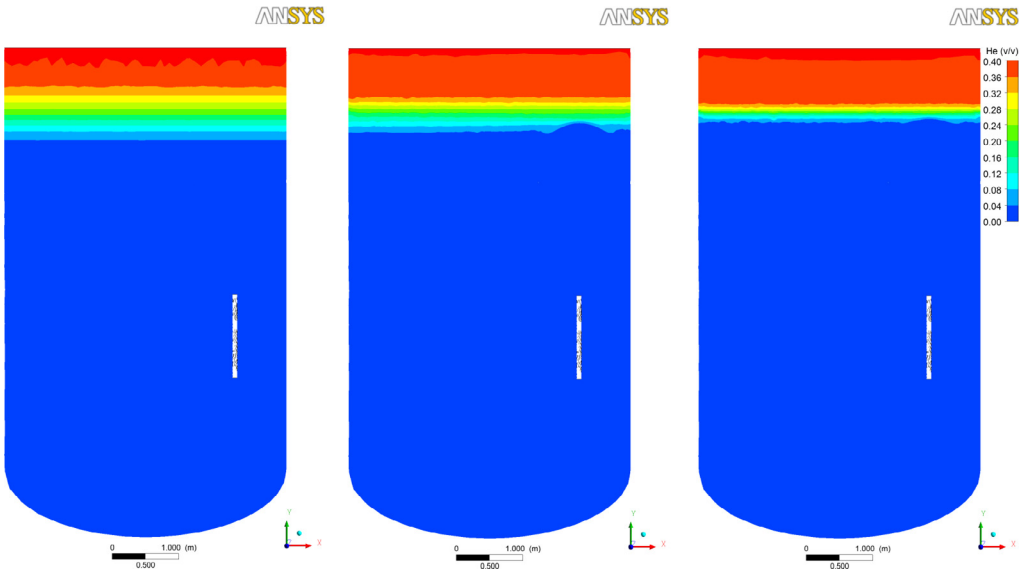

Fig. 13. Centre plane helium concentration predictions from simulation MV3 of LOWMA_3a at t = 0, 60 and 120 s (left to right).

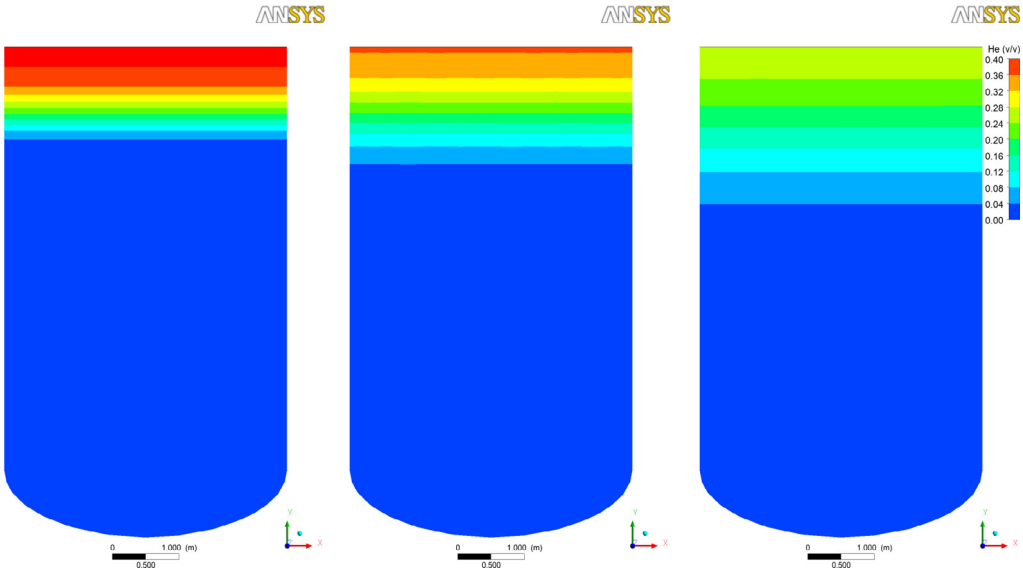

Fig. 14. Centre plane helium concentration predictions from simulation MV4 of INITIALA_3 at t = 0, 1800 and 7200 s (left to right).

where ΔH_{H2} is the heat released by the recombination process and cp_{in} is the specific heat capacity of the gas entering the PAR unit. Eq. (8) assumes that all of the energy released by the recombination process heats the gas (i.e. there is no heating of the PAR unit).

The recombination rate in Eqs. (3-7) was modelled using the AREVA correlation (e.g. Kudriakov et al., 2008; Kotouc, 2012),

$$\dot{r}_{H2} = (k_1 p + k_2) \times \tan h(100 \times c_{H2in} - 100 \times 0.005\ \text{v/v}) \times \min(100 \times c_{H2in}, 100 \times 0.08\ \text{v/v}) \times \mu \times \lambda \quad (9)$$

In Eq. (9) $\dot{r}_{H2}$ is the recombination rate in g/s, the constants k_1 = 0.0137 and k_2 = 0.0163 are suitable for a half FR-380 PAR unit, p is the local pressure in bar and c_{H2in} is the hydrogen molar fraction at the PAR inlet in v/v. The function μ ensures no recombination takes place if the hydrogen concentration is less than 0.005 v/v:

$$c_{H2in} < 0.005\ \text{v/v} \Rightarrow \mu = 0$$

$$c_{H2in} \geqslant 0.005\ \text{v/v} \Rightarrow \mu = 1$$

The function λ defines how the PAR performs if the oxygen concentration, c_{O2in}, is limited:

$$c_{O2in} < 0.0025\ \text{v/v} \Rightarrow \lambda = 0$$

$$c_{O2in} < c_{H2in} \Rightarrow \lambda = 0.6$$

$$c_{O2in} > c_{H2in} \Rightarrow \lambda = 1$$

In all of the simulations described here it was assumed that there was a plentiful supply of oxygen such that $\lambda = 1$.

Fig. 19 illustrates the relationship between the recombination rate, hydrogen concentration and pressure (defined by Eq. (9)) for a range of values relevant to the analyses presented here (in the simulations presented below the pressure was initially 1.0 bar and increased up to 1.6 bar as hydrogen was recombined). The recombination rate increases with increasing pressure and, for hydrogen concentrations below 0.08 v/v, it decreases as the hydrogen concentration drops.

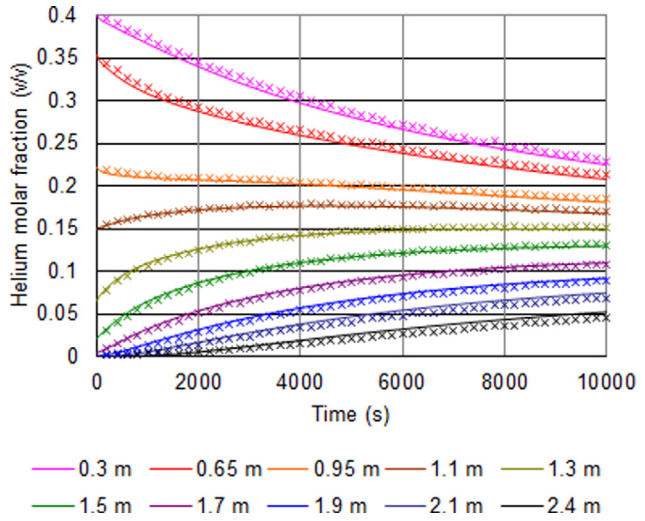

Fig. 15. Helium concentration measurements from INITIALA_3 (crosses) and predictions from simulation MV4 (lines).

6. Results and discussion

The equations for hydrogen recombination were incorporated into the CFD model and a number of verification simulations were carried out to confirm that they had been implemented correctly. The model was then used to simulate a series of four hypothetical scenarios with high or low PAR positions and homogeneous or stratified initial hydrogen distributions. A summary of the simulations and predictions is provided in Table 3.

For the homogeneous simulations the initial hydrogen concentration was 0.1 v/v throughout the vessel and for the stratified simulations the initial concentration was 0.16 v/v above 4 m and zero below 4 m. Both distributions correspond to an initial mass of hydrogen of about 500 g.

Fig. 20 shows hydrogen concentration predictions after 300 s from each of the four simulations. Each simulation develops a unique stratification pattern with a maximum concentration close to the initial concentration. In simulations HR1, HR2 and HR3 warm hydrogen-lean gas accumulates above the PAR inlet, whilst cool hydrogen-rich gas becomes trapped below. In simulation HR2 the cool hydrogen-rich gas becomes sandwiched above a layer of cool air resulting in a three-layer stratification pattern. In simulation HR4 no recombination takes place as the hydrogen-rich gas remains above the PAR inlet (the simulation demonstrates that molecular diffusion alone is not able to mix the atmosphere sufficiently to lead to hydrogen recombination in this scenario).

Similar stratification phenomena have been observed by Reinecke et al. (2013) who carried out simulations of hydrogen recombination in a garage-sized enclosure. However, whilst Reinecke et al. (2013) observed only favourable effects of stratification the results presented here indicate the possibility of both favourable and adverse effects.

Figs. 21 and 22 show predictions for the recombination rate and the total mass of hydrogen left in the THAI vessel from each of the four simulations. The recombination rate is strongly dependant on

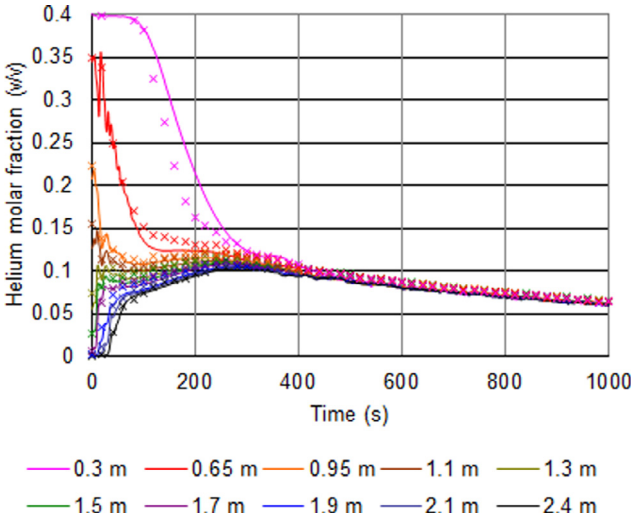

Fig. 17. Helium concentration measurements from LOWMA_4 (crosses) and CFD predictions from MV5 (lines) at sensor locations TCG_0 to TCG_9.

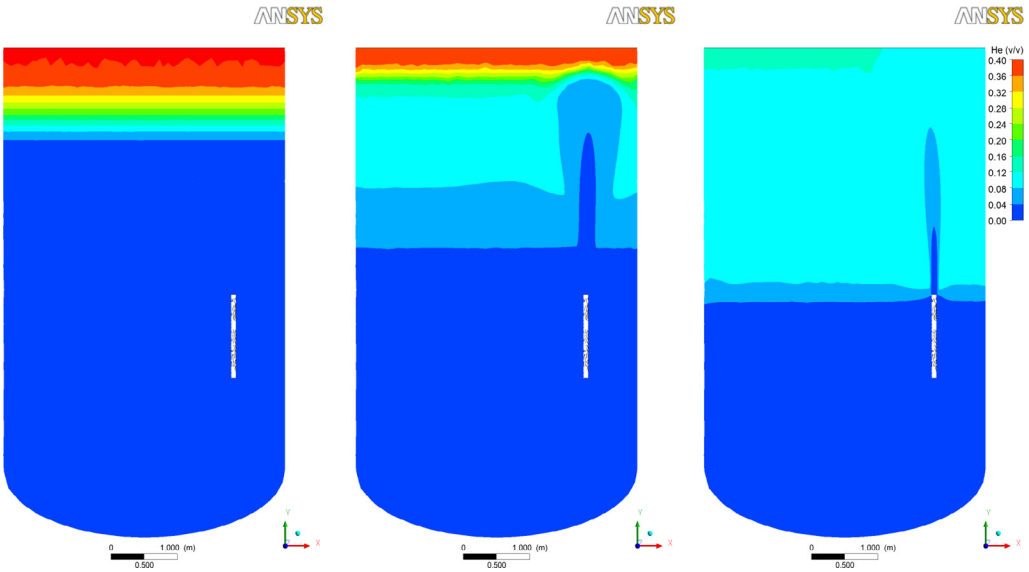

Fig. 16. Centre plane helium concentration predictions from simulation MV5 of LOWMA_4 at t = 0, 120 and 300 s (left to right).

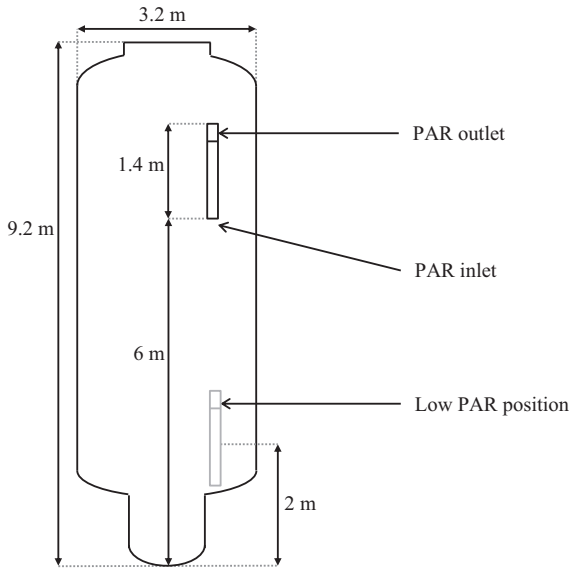

Fig. 18. Schematic of the THAI facility and PAR unit.

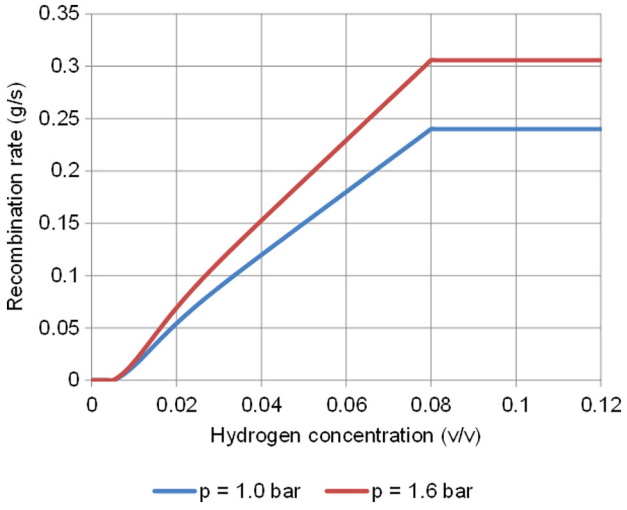

Fig. 19. Recombination rate dependency on hydrogen concentration and pressure.

the hydrogen concentration at the PAR inlet. For example, Fig. 20 shows that at 300 s HR2 and HR3 have the highest PAR inlet hydrogen concentrations and Fig. 21 shows that they have the highest recombination rates. At 300 s HR1 has a lower inlet concentration and a lower recombination rate, whilst HR4 has an inlet concentration and recombination rate of zero.

Recombination rate predictions from simulations HR1, HR2 and HR3 initially increase as the pressure inside the THAI vessel increases. There then follows a sudden decrease in recombination rate as and when the PAR inlet hydrogen concentration drops below 0.08 v/v. This occurs after 150 s in HR1, whilst in HR2 and HR3 it occurs after 280 s and 450 s, respectively.

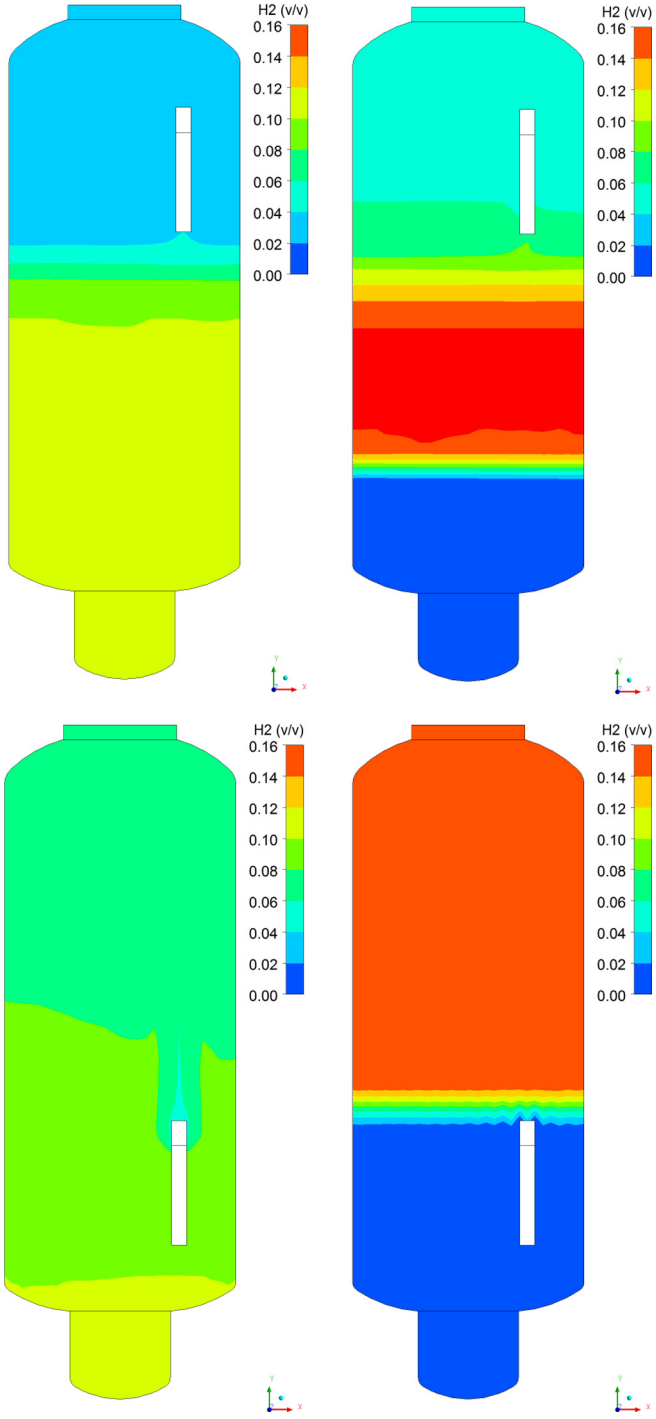

Fig. 20. Centre plane hydrogen concentration predictions at t = 300 s from simulations HR1 (top left), HR2 (top right), HR3 (bottom left) and HR4 (bottom right).

The differences in recombination rate are reflected in the predictions for the total mass of hydrogen left in the THAI vessel. In simulation HR4 there is no recombination and the hydrogen mass remains at 500 g. Conversely, recombination in simulations HR1

Table 3
Overview of PAR performance simulations and predictions.

Simulation	PAR position	Initial hydrogen distribution	Initial hydrogen concentration	Qualitative level of PAR performance
HR1	High	Homogeneous	0.10 v/v	Moderate
HR2	High	Stratified	0.16 v/v above 4 m	Moderate
HR3	Low	Homogeneous	0.10 v/v	Good
HR4	Low	Stratified	0.16 v/v above 4 m	Poor

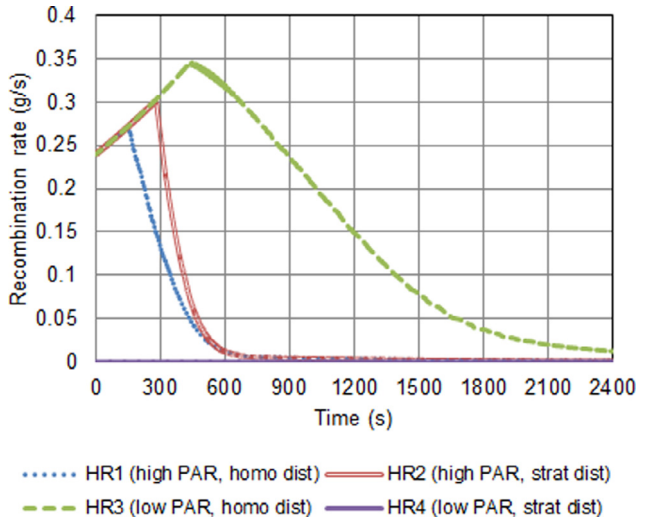

Fig. 21. Recombination rate predictions from CFD simulations with homogeneous and stratified initial hydrogen distributions and high and low PAR positions.

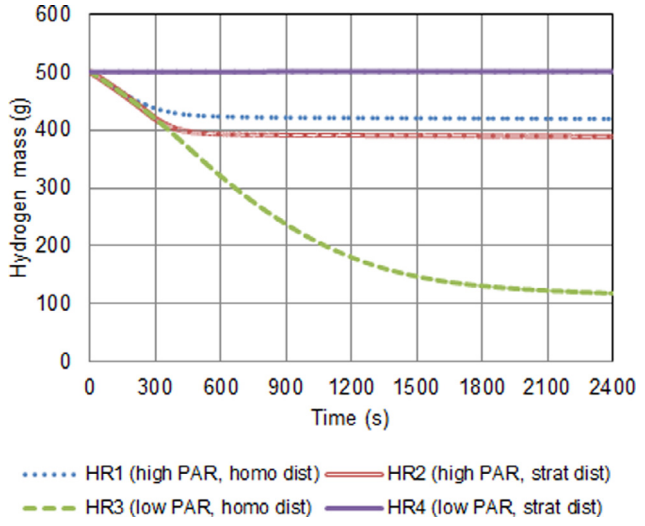

Fig. 22. Hydrogen mass predictions from CFD simulations with homogeneous and stratified initial hydrogen distributions and high and low PAR positions.

and HR2 reduces the total hydrogen mass to 420 g and 390 g, whilst in HR3 the hydrogen mass decreases to 120 g.

The mass of hydrogen left in the vessel provides a useful means of comparing PAR performance in the different simulations. Overall, for the homogenous initial distribution the low PAR outperforms the high PAR whereas for the stratified initial distribution the high PAR outperforms the low PAR.

7. Conclusions

A CFD model has been validated against measurement data for hydrogen dispersion and diffusion in a stably stratified flow from the MISTRA experiments. The model has then been used to simulate a series of hypothetical scenarios involving hydrogen recombination in a large-scale vessel including a model of an AREVA PAR unit. The results provide insight into the use of CFD for safety analyses but also highlight the need for model validation.

The current model was validated against measurements from a series of MISTRA experiments carried out by CEA. These experiments provide useful data for CFD model validation because the initial and boundary conditions are well defined and measurement repeatability is well documented. Furthermore, the measurements have a high spatial and temporal resolution.

Overall, the CFD predictions were in good agreement with the experimental measurements. However, the model was found to be very sensitive to the mesh type with predictions from simulations carried out on tetrahedral meshes being in poor agreement with the measurements. It is widely known that the use of tetrahedral meshes can lead to unphysical numerical diffusion that can result in mixing being over-predicted. However, contrary to this, the simulations presented here using the tetrahedral mesh led to small unphysical convection currents that resulted in mixing being under-predicted.

This is an important result from the perspective of CFD model reliability, since it is often assumed that CFD simulations using tetrahedral meshes will over-predict mixing, whereas these results show that the opposite is possible. Other versions of CFX and other CFD codes are likely to be affected by this issue. This issue is not described in current best practice guidelines. However, following advice on mesh sensitivity analyses and verification and validation, including advice on adopting a tiered approach (NEA, 2015), will help to identify any potential unphysical effects. As an additional precaution, consideration should be given to using gravity-aligned meshes for modelling stratified flows.

The simulations of hydrogen recombination were carried out using gravity-aligned meshes and a relatively simple PAR model that can be used for containment or ventilation applications. Four hypothetical scenarios were simulated with uniform and stratified initial hydrogen distributions and with high and low PAR positions. The results show that the performance of a PAR unit depends on its position and the distribution of hydrogen gas. For a homogeneous initial hydrogen distribution a low PAR location performed better than a high PAR but for a stratified initial hydrogen distribution a high PAR performed better than a low PAR. The differences between the performances of the PAR units in these different cases highlights the importance of using a model that can take into account the effect of the hydrogen stratification.

The scenarios considered here were highly simplified in comparison to real scenarios, which could involve condensation, elevated pressures and temperatures, a continuous release of hydrogen, multi-room geometries and multiple PAR units. To apply a CFD model to these more realistic cases would require a wider ranging validation study to be undertaken, encompassing other key physics affecting PAR performance, such as thermally-driven natural convection currents. In this study the emphasis has been on stratification phenomena and involved first validating the model for stratification in the presence of different strength *mechanically-driven* convection currents and then using it to investigate stratification effects on PAR performance.

In a real scenario the relationship between the position of a PAR unit and its performance could be complex. The use of CFD to optimise the position of PAR units in an enclosure is anticipated to be a practicable measure to increase the performance of PAR units and thus reduce the hydrogen-hazard in the event of a severe accident in a nuclear power plant.

Disclaimer

This publication and the work it describes were co-funded by the Health and Safety Executive (HSE) and the Office for Nuclear Regulation (ONR). Its contents, including any opinions and/or conclusions expressed, are those of the authors alone and do not necessarily reflect HSE or ONR policy.

Acknowledgment

The authors would like to thank Ali Tehrani, Office for Nuclear Regulation, for helping to steer the research described here and commenting on an early draft of the paper.

References

Agrawal, N., Prabhakar, A., Das, S.K., 2015. Hydrogen distribution in nuclear reactor containment during accidents and associated heat and mass transfer issues—a review. Heat Transfer Eng. 36 (10), 859–879.

Allelein, H.J., Arndt, S., Klein-Heßling, W., Schwarz, S., Spengler, C., Weber, G., 2008. COCOSYS: status of development and validation of the German containment code system. Nucl. Eng. Des. 238 (4), 872–889.

ANSYS, 2011. ANSYS CFX-Solver Theory Guide. ANSYS Inc., Southpointe, 275 Technology Drive, Canonsburg, PA 15317. Release 14.0, November 2011.

AREVA, 2011. AREVA Passive Autocatalytic Recombiner. Severe Accident-Qualified PAR for Combustible Gas Control. G-008-V1PB-2011-ENG, AREVA Inc., Bethesda, US.

Bird, R.B., Stewart, W.E., Lightfoot, E.N., 1960. Transport Phenomena. John Wiley and Sons Inc., New York.

Brinster, J., Abdo, D., Studer, E., Tkatschenko, I., Widloecher, J.L., 2009. OECD/SETH2 Project: Synthesis Report for MISTRA INITIALA/LOWMA Tests. CEA Technical Report.

Brinster, J., Studer, E., Tkatschenko, I., 2011. Short Description of MISTRA Facility for Air-Helium Mixing Tests. CEA Technical Report.

Crank, J., 1975. The Mathematics of Diffusion. Oxford University Press, Oxford.

EC, 2012. Communication from the Commission to the Council and the European Parliament on the Comprehensive Risk and Safety Assessments ("Stress Tests") of Nuclear Power Plants in the European Union and Related Activities. European Commission, Brussels, October 2012.

Gupta, S., 2015. Experimental investigations relevant for hydrogen and fission product issues raised by the Fukushima accident. Nucl. Eng. Technol. 47 (1), 11–25.

Hedley, D., Hawksworth, S.J., Rattigan, W., Brentnall, R., Allen, J., 2014. Large scale passive ventilation trials of hydrogen. Int. J. Hydrogen Energy 39 (35), 20325–20330.

Hooker, P., Hoyes, J.R., Hall, J., Willoughby, D., 2015. Experimental studies on vented deflagrations in a low strength enclosure. In: The 6th International Conference on Hydrogen Safety, 19–21 October 2015. Yokohama, Japan.

Hoyes, J.R., Ledin, H.S., Tehrani, A.A.K., 2013. Benchmarking on hydrogen deflagrations ISP-49: CFD modelling capabilities and limitations. The 15th International Topical Meeting on Nuclear Reactor Thermal Hydraulics, 12–15 May 2013. Pisa, Italy.

IAEA, 2011. Mitigation of Hydrogen Hazards in Severe Accidents in Nuclear Power Plants, International Atomic Energy Agency, Vienna, 2011. IAEA-TECDOC-1661.

Kanzleiter, T., 2009. Quick Look Report: Hydrogen Recombiner Tests HR-1 to HR-5, HR-27 and HR-28 (Tests without steam). Reactor Safety Research Project 150 1326, OECD/NEA THAI Project Report No. 150 1326-HR-QLR-1, Becker Technologies GmbH, Eschborn, Germany, February 2009.

Kljenak, I., Kuznetsov, M., Kostka, P., Kubišova, L., Manzini G., Povilaitis, M., 2013. Simulation of Hydrogen Deflagration Experiment – Benchmark Exercise with Lumped-Parameter Codes. The 22nd International Conference on Nuclear Energy for New Europe. 9–12 September 2013. Bled, Slovenia.

Kotouc, M., 2012. Validation of the LP code Melcor 1.8.6 for containment analyses with hydrogen recombiners using results from the OECD/NEA experimental project THAI. In: Proceedings of the 20th International Conference on Nuclear Engineering. 30th July – 3rd August 2012. Anaheim, California, USA.

Kudriakov, S., Dabbene, F., Studer, E., Beccantini, A., Magnaud, J.P., Paillère, H., Bentaib, A., Bleyer, A., Malet, J., Porcheron, E., Caroli, C., 2008. The TONUS CFD code for hydrogen risk analysis: physical models, numerical schemes and validation matrix. Nucl. Eng. Des. 238 (3), 551–565.

Kuznetsov, M., Yanez, J., Grune, J., Friedrich, A., Jordan, T., 2015. Hydrogen combustion in a flat semi-confined layer with respect to the Fukushima Daiichi accident. Nucl. Eng. Des. 286, 36–48.

Lewis, B., von Elbe, G., 1961. Combustion, Flames and Explosions of Gases. Academic Press, New York.

Meynet, N., Bentaib, A., 2012. Numerical study of hydrogen ignition by passive autocatalytic recombiners. Nucl. Technol. 178 (1), 17–28.

NEA, 2007. International Standard Problem ISP-47 on Containment Thermal Hydraulics, Final Report. NEA/CSNI/R(2007) 10.

NEA, 2011. ISP-49 on Hydrogen Combustion. NEA/CSNI/R(2011) 9.

NEA, 2012. OECD/SETH-2 Project PANDA and MISTRA Experiments Final Summary Report. Investigation of Key Issues for the Simulation of Thermal-Hydraulic Conditions in Water Reactor Containment. NEA/CSNI/R(2012) 5.

NEA, 2013. The Fukushima Daiichi Nuclear Power Plant Accident: OECD/NEA Nuclear Safety Response and Lessons Learnt. NEA No. 7161.

NEA, 2015. Best Practice Guidelines for the use of CFD in Nuclear Reactor Safety Applications – Revision. NEA/CSNI/R(2014) 11.

NRA, 2014. Analysis of the TEPCO Fukushima Daiichi NPS Accident, Interim Report by Nuclear Regulatory Authority, Japan, October 2014.

ONR, 2011. Generic Design Assessment – New Civil Reactor Build. Step 4 Reactor Chemistry Assessment of the EDF and AREVA UK EPR Reactor. Assessment Report: ONR-GDA-AR-11-024, Revision 0, November 2011.

ONR, 2012. Japanese Earthquake and Tsunami: Implementing the Lessons for the UK's Nuclear Industry. ONR Fukushima Implementation Report: ONR-FR-REP-12-001 Revision 0, October 2012.

Paladino, D., Andreani, M., Zboray, R., Dreier, J., 2012. Toward a CFD-grade database addressing LWR containment phenomena. Nucl. Eng. Des. 253, 331–342.

Reinecke, E.A., Kelm, S., Jahn, W., Jäkel, C., Allelein, H.J., 2013. Simulation of the efficiency of hydrogen recombiners as safety devices. Int. J. Hydrogen Energy 38 (19), 8117–8124.

Sathiah, P., Komen, E., Roekaerts, D., 2015. The role of CFD combustion modeling in hydrogen safety management–III: Validation based on homogeneous hydrogen–air–diluent experiments. Nucl. Eng. Des. 289, 296–310.

Sellafield, 2015. Risk and Hazard Reduction: Magnox Swarf Storage Silos <http://www.sellafieldsites.com/solution/risk-hazard-reduction/magnox-swarf-storage-silos/> (accessed 10th July 2015).

Studer, E., Brinster, J., Tkatschenko, I., Mignot, G., Paladino, D., Andreani, M., 2012. Interaction of a light gas stratified layer with an air jet coming from below: large scale experiments and scaling issues. Nucl. Eng. Des. 253, 406–412.

TEPCO, 2012. Fukushima Nuclear Accident Analysis Report, Tokyo Electric Power Company Inc, June 2012.

Visser, D.C., Houkema, M., Siccama, N.B., Komen, E.M.J., 2012. Validation of a FLUENT CFD model for hydrogen distribution in a containment. Nucl. Eng. Des. 245, 161–171.